Fuel 303 (2021) 121240

Contents lists available at ScienceDirect

Fuel

journal homepage: www.elsevier.com/locate/fuel

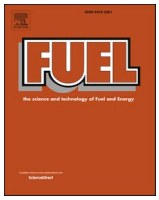

Full Length Article

A reactor-scale CFD model of soot formation during high-temperature pyrolysis and gasification of biomass

Tao Chen [a,*], Tian Li [b,c], Jonas Sjöblom [a], Henrik Ström [a,c]

[a] Department of Mechanics and Maritime Sciences, Chalmers University of Technology, 41296 Göteborg, Sweden
[b] RISE Fire Research, NO-7092 Tiller, Norway
[c] Department of Energy and Process Engineering, Norwegian University of Science and Technology, 7491 Trondheim, Norway

ARTICLE INFO

Keywords:
Soot formation
Biomass gasification
Two-equation model
Eulerian-Lagrangian

ABSTRACT

Soot generation is an important problem in high-temperature biomass gasification, which results in both air pollution and the contamination of gasification equipment. Due to the complex nature of biomass materials and the soot formation process, it is still a challenge to fully understand and describe the mechanisms of tar evolution and soot generation at the reactor scale. This knowledge gap thus motivates the development of a comprehensive computational fluid dynamics (CFD) soot formation algorithm for biomass gasification, where the soot precursor is modeled using a component-based pyrolysis framework to distinguish cellulose, hemicellulose and lignin. The model is first validated with pyrolysis experiments from different research groups, after which the soot generation during biomass steam gasification in a drop-tube furnace is studied under different operating temperatures (900–1200 °C) and steam/biomass ratios. Compared with the predictions based on a detailed tar conversion model, the current algorithm captures the soot generation more reasonably although a simplified tar model is used. Besides, the influence of biomass lignin content and the impact of tar and soot consumptions on the soot yield is quantitatively studied. Moreover, the impact of surface growth on soot formation is also discussed. The current work demonstrates the feasibility of the coupled multiphase flow algorithm in the prediction of soot formation during biomass gasification with strong heat/mass transfer effects. In conclusion, the model is thus a useful tool for the analysis and optimization of industrial-scaled biomass gasification.

1. Introduction

Biomass gasification is one of the most promising technologies that plays an important role in the energy supply system of many countries [1–3]. However, there are still some practical issues (e.g., tar generation) in industrial-scale biomass utilization [4–6]. Among various ways of improving the conversion efficiency, high-temperature operation and pulverization of the feedstock are the most commonly used strategies such as in entrained flow gasification [7,8]. Moreover, increasing the operating temperature results in additional problems, in particular soot formation, which has an adverse impact on the subsequent cleaning of the bio-syngas and in the maintenance of the gasification equipment [9]. Besides, the overall cold-gas efficiency decreases due to the formation of the carbon-rich soot particles. Therefore, understanding the mechanism of soot formation is important.

The soot formation process during biomass gasification is similar to the situation in internal combustion engines, which generally follows the route of precursor formation, the inception of initial soot particles and finally the growth and coagulation of larger soot particles [10]. The uniqueness of biomass soot generation is mainly due to the difference in the formation of soot precursors, which is determined to a large extent by the tar generation [11–13], i.e. tar evolution is the basis of soot formation. However, unlike soot generation, which usually happens under high-temperature conditions (above 1000 °C), tar generation is observed at relatively much lower operating temperatures such as 400–500 °C. With the increase of temperature (above 600–800 °C), the primary tar species undergo thermal cracking, forming secondary and tertiary tars [14]. Under higher temperatures, these tar species (e.g. phenol) will further convert to complex ring structures, i.e., soot precursors [9,15]. Therefore, in the development of models for tar and soot in biomass gasification, the difference in the formation mechanism, especially the temperature-dependent character, is a key issue.

In the last few decades, many different tar models were established for biomass pyrolysis and gasification. Palma [16] as well as Gómez-Barea and Leckner [17] have made comprehensive reviews on this issue

* Corresponding author.
E-mail address: tchen@chalmers.se (T. Chen).

https://doi.org/10.1016/j.fuel.2021.121240
Received 16 March 2021; Received in revised form 11 May 2021; Accepted 8 June 2021
Available online 17 June 2021

Nomenclature

A_i	pre-exponential factor, s/m
A_p	surface area of biomass particle, m^2
c_p	specific heat of biomass particle, J/(kg K)
C_i	gas phase mass diffusion rate in Eq. 3, $s/K^{0.75}$
D_{eff}	effective mass diffusion coefficient, m^2/s
d_p, d_s	diameter of char particle and soot particle, m
e_p	emissivity, -
E_i	activation energy, J/mol
G	incident radiation, kg/s^3
h	heat transfer coefficient, $W/(m^2 K)$
h_{sen}	sensible enthalpy, J/kg
m_p	mass of biomass particle, kg
$m_{C\text{-}i}$	char mass, kg
N	number of soot particles, -
p_i	partial pressure, Pa
Q_p	energy source term, W/m^3
$r_{diff,i}$	diffusion rates, m/s
$r_{kin,i}$	kinetic rates, m/s
S_h	reaction enthalpy, W/m^3
$S_{p,m}$	mass source term from particle, $kg/(m^3 s)$
$S_{p,h}$	enthalpy source term from particle, W/m^3
S_{rad}	energy source term of radiation, W/m^3
$S_{p,Yi}$	species source term from particle, $kg/(m^3 s)$
S_{Yi}	species source term from reactions, $kg/(m^3 s)$
$S_{p,mom}$	momentum source term, N/m^3
T_g, T_p	gas phase and particle temperature, K
$\boldsymbol{v}_p$	velocity of biomass particle, m/s
Y_i	mass fraction of gas species i, -
α_{eff}	effective thermal diffusivity, kg/(m s)
σ	Stefan-Boltzmann constant, $W/(m^2 K^4)$
$\boldsymbol{\tau}_{eff}$	effective stress tensor, Pa

and Wang et al. also discussed the recent progress [18]. The simplest tar model lumps tar species as a single compound with or without giving its specific chemical formalisms [19]. Although it is difficult to determine the global reaction kinetics related to tar evolution for the simple tar model, a straightforward concept can be easily obtained in terms of the competition between tar formation and consumption. The second type of tar model can be represented by the multistep pyrolysis mechanism [20–23]. It is a semi-detailed model where tar is simplified with several chemical species such as C_3H_6O, C_6H_6O and $C_{11}H_{12}O_4$. Finally, the detailed models account for tar species and the corresponding reaction schemes as realistically as possible[24] . Besides converting to soot precursors, tar can also react with oxidants such as steam and carbon dioxide during gasification [25,26]. The competition between tar conversion and consumption makes it difficult to accurately model soot formation due to the wide distribution of tar species. The uncertainty faced in establishing the reaction kinetics of all the different tar species is still a big challenge[27] , especially for semi-detailed and detailed tar models, where the large number of elemental tar reactions involved inhibits their implementation in complex computational fluid dynamics (CFD) simulations.

Another challenge in the modeling of soot formation is related to the formation process of soot particles[28] . Existing studies have shown that the growth of soot particles follows a complex procedure [9,29,30], including inception, coagulation, surface growth and oxidation, during which there is also a small amount of hydrogen released from the soot particle. As a result, the size of soot particles has a wide distribution depending on temperature and the surrounding gas-phase environment [31] . Besides, the morphology of a soot particle, which is usually observed as having an onion-like structure[32] , also has a close relationship with temperature and its trajectory history[33] . These unique internal structures of soot particles make it difficult to develop a uniform soot consumption mechanism. Recently, Morán et al. studied the coupled effect of surface growth and coagulation during soot formation [34] . They found that the surface growth changes both the morphology and residence time of the soot particles resulting in a slowing down of the coagulation process. Davis et al. observed that, for matured soot particles, voids can be formed inside the core–shell structure during the oxidation process, which cause a significant influence on the reactivity of the soot particles[35] . Chang et al. found that oxidants can penetrate the core–shell structure inside the soot particle, which results in a different way of consumption compared with the regime of surface oxidation[36] .

Besides the above-mentioned difficulties, modeling of soot formation for biomass gasification also needs to deal with several other issues, such as the variations of fuel type, operating condition and the catalytic effect caused by alkali metals in biomass [37–39]. Therefore, it is still a big challenge to establish a comprehensive soot formation model without simplifications on tar evolution and soot conversion. In recent years, some interesting progress on soot modeling for solid fuels are found. Brown and Fletcher made an early attempt on soot modeling for coal gasification/combustion[40] . Josephson et al. developed a detailed kinetic model of soot formation that is applicable for both biomass and coal based on the chemical percolation devolatilization (CPD) pyrolysis model, where the soot precursor is lumped as four basic carbohydrates (C_6H_6O, C_6H_6, C_7H_8 and $C_{10}H_8$), and the subprocesses, including surface growth, consumption, nucleation and coagulation, are all modeled using collisional theory[41] . The model is believed to reproduce experimental results quite well for both soot mass fraction and particle size distribution. However, in their model, the determination of the precursor mole fraction is rather case-dependent in terms of different fuel types and operating temperatures, which makes it difficult to implement. To solve this problem, Niksa established a detailed soot formation model based on the FLASHCHAIN pyrolysis model, which is applicable for any type of coal and biomass[42] . Recently, Ferreiro et al. also developed a soot kinetic mechanism with a competitive multistep biomass pyrolysis model[43] . The mechanism achieves good performance under different operating temperatures and steam/biomass ratios due to the comprehensive consideration of tar conversions. However, information on the soot particle size distribution is not accounted for in these studies [42] [43].

Since the soot formation process is highly dependent on temperature and gas-phase convection (the combination of which determines the evolution of the particle properties), it is necessary to couple soot kinetics with flow field evolution in numerical simulations. Among various types of reactor-scale soot modeling, Xu et al. studied the coupling effect of soot formation with flow field evolution during pulverized coal combustion in a jet burner, where both soot mass fraction and the number density of soot particles are resolved[44] . The soot agglomeration is found to have a close relationship with flame temperature, which, in turn, is influenced by the soot formation. In the coupled CFD and soot formation simulation, the soot volume fraction is well predicted by using Brown and Fletcher's kinetic mechanism[40] . However, the soot particle size distribution is not reported in their work. Muto et al. also established a coupled CFD and soot formation algorithm for a coal gasifier based on Unsteady Reynolds Averaged Navier Stokes (URANS) simulation[45] , in which a two-equation soot model is adopted to describe the evolution of soot mass fraction and particle size. The soot mass distribution is found to have a maximum in the area between the peak flame temperature and the unburned volatile temperature due to the coupled effect of turbulence and chemical reaction. The

relationship between soot formation and coal particle distribution is also studied. Recently, Takahashi et al. developed a numerical algorithm for the study of a 4 kW pulverized coal burner with a combined large eddy simulation (LES) and Brown and Fletcher's two-equation soot model [46] . It is shown that the concentration of the gasifying agent and the soot particle diffusion have important influences on the soot-formation rate near the flame region.

The above discussions illustrate that reactor-scale soot modeling algorithms have been established based on both URANS and LES, and that the two-equation model is one of the most widely used approaches for the modeling of soot formation from solid fuels. However, these reactor-scale soot modeling works have mainly been carried out for coal gasification. When it comes to biomass, some extra difficulties are encountered which are mainly caused by the complex nature of biomass material and hence its tar evolutions. As a result, reactor-scale soot modeling for biomass gasification is still rare [9]. This paper aims to establish a simple and comprehensive reactor-scale model that includes the main features of the biomass primary pyrolysis, tar evolution and soot formation by coupling an Eulerian-Lagrangian algorithm with a two-equation soot model, which is also the main novelty of the current work. The method developed here can be a useful tool for the design and optimization of gasifiers. The paper is organized as follows: Section 2 introduces the modeling of biomass gasification and the kinetics of soot formation as well as the coupled multiphase flow algorithm. Simulation results are shown in Section 3. Then, some further discussions are made in Section 4. Finally, conclusions are drawn in Section 5.

2. Methodology

Under high temperatures, biomass undergoes moisture evaporation and then volatile release, where tar species is a key factor that influences the formation of polycyclic aromatic hydrocarbons (PAH). Following the conversion of PAHs to soot precursors, initial soot particles are generated from the nucleation of precursors. Then surface growth and agglomeration happen, which finally results in a distributed size of mature soot particles. In the presence of a gasifying agent such as air and/or steam, competing reactions also exist in tar consumption, and conversions of precursors and soot particles. So far, there have been many soot formation algorithms with varying complexity in terms of tar conversion and soot evolution[47] , among which the hydrogen abstraction and carbon addition (HACA) mechanism is one of the most commonly used routes in numerical simulations[48] . However, it is also noted that significant variations in the kinetics exist in different soot models for biomass gasification/combustion. For example, the soot precursor used in different models differs from acetylene to more complex ring structures such as benzene and naphthalene[49] , which usually require different kinetics of tar evolution. As a result, the nucleation rate also varies a lot in different soot models [50,51]. Besides, in the case of gasification and combustion, the oxidation rate of soot can have different expressions depending on whether the size distribution of soot particles is considered or not [43,49]. Moreover, for biomass gasification, soot formation is usually studied separately from that of the flow field evolution, which is far from the requirement of industrial-scale analysis with complex turbulence-reaction interactions. Therefore, it is necessary to establish a simplified and comprehensive algorithm that integrates the key models including flow-field evolution, pyrolysis, tar evolution and soot formation.

2.1. Biomass gasification model

In the last few decades, many pyrolysis models have been established. One of the most widely used method is the simplified global reaction model, where the stoichiometric coefficient of each volatile species is prescribed. There are also more complex pyrolysis models such as semi-detailed and detailed pyrolysis models, in which different pyrolysis routes are considered and the primary tar generation, secondary tar cracking and even tertiary tar conversion are modeled with a high level of detail [21,24]. However, the tar evolution process is rather complex and a uniform tar model is still unavailable to the best of the authors' knowledge. Assumptions are still needed for tar species in semi-detailed and even detailed biomass pyrolysis models, which inevitably introduces significant uncertainty in the kinetic constants. For gasification, extra oxidation reactions need to be considered, implying that the uncertainty is further amplified. Therefore, in the modeling of soot formation, it is a good choice to use a simplified global type pyrolysis model where the uncertainty can be easily analyzed. In this paper, we choose a one-step first-order Arrhenius type model to solve the pyrolysis of biomass, where tar species is lumped as a single compound $C_6H_{6.2}O_{0.2}$[52] . To make it a general model applicable for different biomass materials, we consider the pyrolysis of the three basic components of cellulose ($C_6H_{10}O_5$), hemicellulose ($C_5H_8O_4$) and lignin (composed of $C_{15}H_{14}O_4$, $C_{20}H_{22}O_{10}$, and $C_{22}H_{28}O_9$)[21] . For each biomass, the pyrolysis simulation is implemented by using the combination of the pyrolysis of the three basic components[23] . Table 1 lists the pyrolysis models for cellulose, hemicellulose, and lignin, which are derived by the method of ensuring the mass conservation of the basic elements of C, H, and O as has been used in our previous work[53] .

Biomass = a1 $C_6H_{10}O_5$ + a2 $C_5H_8O_4$ + a3 $C_{15}H_{14}O_4$ + a4 $C_{20}H_{22}O_{10}$ + a5 $C_{22}H_{28}O_9$where, the mass fraction 'ai' ($i = 1, 2\ldots5$) of each biomass component can be obtained from experiments[21] .

The tar evolution includes thermal cracking and gasification reactions. Table 2 lists the chemical reactions of tar evolution. In the tar cracking reaction (R1), the secondary tar is modeled as C_6H_6, which is the only species from which soot inception occurs in the present work. During gasification the secondary tar is also consumed with the gasifying agent. The other gas-phase reactions including the gasification of H_2, CH_4 and CO are shown in the supplementary material Table S1. During gasification, the heterogeneous reactions of char particles include the consumption by O_2, CO_2 and H_2O, which are computed with accounting for both diffusion and kinetic effects [54]. The biomass thermochemical conversion process is modeled by using a CFD-DPM (discrete parcel method) multiphase flow algorithm [55]. The governing balance equations for the gas phase and the particle phase are shown in Table 3. In this work, our primary focus is on biomass gasification in drop-tube furnaces, where the gas-particle flow can be treated as a dilute system. Therefore, the influence of particle volume fraction is not considered in the gas-phase governing equations. Besides, the collision between biomass particles is also neglected.

2.2. Soot evolution model

Soot formation has been extensively studied in the literature for gaseous fuels [62]. Therefore, it is a good choice to build on the existing models as has been done for coal combustion considering the similar sub-processes such as soot inception, coagulation and consumption [44–46]. Among various soot modeling algorithms, the two-equation model is one of the most widely used[46] . In this paper, we assume that the transport behavior of soot during biomass gasification is similar to that in gas fuel combustion. The transport governing equations include the soot mass fraction transport equation (Eq. 5 in Table 3) and soot particle number density transport equation (Eq. 6 in Table 3)[45] , where Y_{soot} is the soot mass fraction, M is the soot concentration (kg/m^3). n_{soot} is the normalized number density of soot particles. The non-dimensional parameter N^* is set to 10^{15}[60] , which is used to avoid dealing with large numbers in programing. The production rate of soot is computed by considering the nucleation from the gas-phase precursor (benzene is assumed to be the precursor in this work) and the coagulation of soot particles in the free-molecular regime as shown in Eqs. 7 and 8, where M_p represents the mass of an incipient soot particle. In this work, we assume that an incipient soot particle contains 100 carbon atoms, i.e., M_p equals 1.2 kg/mol [61]. ρ_{soot} is the density of soot particles which is set as 2000 kg/m^3 [45,60]. [X_i] and [X_{prec}] are the mole

Table 1
Biomass component pyrolysis model (biomass component → x1 H_2 + x2 CH_4 + x3 CO_2 + x4 H_2O + x5 Carbon + x6 $C_6H_{6.2}O_{0.2}$).

Component	H_2	CH_4	CO	CO_2	H_2O	Carbon	$C_6H_{6.2}O_{0.2}$	A (1/s)	E (J/mol)
$C_6H_{10}O_5$	2.224	1.25	2.598	1.15	0.09	0.642	0.06	1.3×10^{10}	1.505×10^5
$C_5H_8O_4$	2.069	0.878	2.512	0.7	0.082	0.73	0.03	1.3×10^{10}	1.505×10^5
$C_{15}H_{14}O_4$	2.052	1.21	1.992	0.9	0.048	6.098	0.8	7.7×10^6	1.114×10^5
$C_{20}H_{22}O_{10}$	3.95	2.105	4.6	2.585	0.05	5.31	0.9	7.7×10^6	1.114×10^5
$C_{22}H_{28}O_9$	5.82	2.335	4.18	2.25	0.1	6.635	1.1	7.7×10^6	1.114×10^5

Table 2
Tar and precursor evolution model.

Reaction	Reaction rate	
$C_6H_{6.2}O_{0.2} \rightarrow 0.11\ H_2 + 0.06\ CH_4 + 0.2\ CO + 287/300\ C_6H_6$	$k = 4.28 \times 10^4 [C_6H_{6.2}O_{0.2}] \exp(-1.08 \times 10^5/RT)$	R1 [56,57]
$C_6H_{6.2}O_{0.2} + 2.9\ O_2 \rightarrow 3.1\ H_2 + 6\ CO$	$k = 1.58 \times 10^{15} [C_6H_{6.2}O_{0.2}][O_2] \exp(-2.026 \times 10^5/RT)$	R2 [58,59]
$C_6H_{6.2}O_{0.2} + 3.8\ H_2O \rightarrow 0.9\ H_2 + 2\ CO + CO_2 + 3\ CH_4$	$k = 4.28 \times 10^5 [C_6H_{6.2}O_{0.2}] [H_2O]^{0.2} \exp(-1.08 \times 10^5/RT)$	R3 [49,56]
$C_6H_{6.2}O_{0.2} + 5.8\ CO_2 \rightarrow 3.1\ H_2 + 11.8\ CO$	$k = 4.28 \times 10^5 [C_6H_{6.2}O_{0.2}][CO_2] \exp(-1.08 \times 10^5/RT)$	R4 [56]
$C_6H_6 + 3\ O_2 \rightarrow 3\ H_2 + 6\ CO$	$k = 1.58 \times 10^{15} [C_6H_6][O_2] \exp(-2.026 \times 10^5/RT)$	R5 [58]
$C_6H_6 + 5\ H_2O \rightarrow 6\ H_2 + CH_4 + 5\ CO$	$k = 4.4 \times 10^8 [C_6H_6] \exp(-2.2 \times 10^5/RT)$	R6 [49]

Table 3
Governing equations of the biomass gasification algorithm with soot formation [45,55,60,61].

Submodel	Governing equation
Gas phase	Mass: $\frac{\partial}{\partial t}\rho_g + \nabla\cdot(\rho_g \boldsymbol{u}_g) = S_{p,m}$ (1)
	Momentum: $\frac{\partial}{\partial t}(\rho_g \boldsymbol{u}_g) + \nabla\cdot(\rho_g \boldsymbol{u}_g \boldsymbol{u}_g) = -\nabla p + \nabla\cdot(\boldsymbol{\tau}_{eff}) + \rho_g \boldsymbol{g} + S_{p,mom}$ (2)
	Energy: $\frac{\partial}{\partial t}(\rho_g E) + \nabla\cdot(\boldsymbol{u}_g(\rho_g E + p)) = \nabla\cdot(\alpha_{eff}\nabla h_{sen}) + S_h + S_{p,h} + S_{rad}$ (3)
	Gas species: $\frac{\partial}{\partial t}(\rho_g Y_i) + \nabla\cdot(\rho_g \boldsymbol{u}_g Y_i) = \nabla\cdot(\rho_g D_{eff}\nabla Y_i) + S_{p,Y_i} + S_{Y_i}$ (4)
	Soot: $\frac{\partial}{\partial t}(\rho_g Y_{soot}) + \nabla\cdot(\rho_g \boldsymbol{u}_g Y_{soot}) = \nabla\cdot(D_{eff}\nabla Y_{soot}) + \frac{dM}{dt}$ (5)
	$\frac{\partial}{\partial t}(\rho_g n_{soot}) + \nabla\cdot(\rho_g \boldsymbol{u}_g n_{soot}) = \nabla\cdot(D_{eff}\nabla n_{soot}) + \frac{1}{N^*}\frac{dN}{dt}$ (6)
	$\frac{dM}{dt} = M_p C_\alpha [X_{prec}] exp(-\frac{T_\alpha}{T}) - \sum_{i=1,2,3} C_{\omega i}[X_i] exp(-\frac{T_{\omega i}}{T}) T^{0.5} (\pi N)^{\frac{1}{3}} \left(\frac{6M}{\rho_{soot}}\right)^{\frac{2}{3}}$ (7)
	$\frac{dN}{dt} = C_\alpha N_A [X_{prec}] exp(-\frac{T_\alpha}{T}) - C_\beta \left(\frac{24RT}{\rho_{soot} N_A}\right) d_s^{0.5} N^2$ (8)
Particle phase	Mass: $\frac{dm_p}{dt} = \frac{dm_{vapor}}{dt} + \frac{dm_{devol}}{dt} + \frac{dm_{C-O_2}}{dt} + \frac{dm_{C-CO_2}}{dt} + \frac{dm_{C-H_2O}}{dt}$ (9)
	Momentum: $m_p \frac{dv_p}{dt} = f_g + m_p g$ (10)
	Energy: $m_p c_p \frac{dT_p}{dt} = hA_p(T_g - T_p) + \frac{e_p A_p}{4}(G - 4\sigma T_p^4) + Q_p$ (11)
	Drag correlation: $f_g = \frac{3\mu_g C_d Re_p}{4\rho_p d_p^2}(\mathbf{u}_g - \mathbf{v}_p)$
	$C_d = \begin{cases} \frac{24}{Re_p}(1 + 0.15 Re_p^{0.687}) & Re_p < 1000 \\ 0.44 & Re_p \geqslant 1000 \end{cases}$ (12)
	$Re_p = \rho_g d_p \lvert \mathbf{u}_g - \mathbf{v}_p \rvert / \mu_g$

concentrations of gasification agents (O_2, CO_2 and H_2O) and soot precursor. N_A is the Avogadro number, which is 6.022×10^{23} mol^{-1}. The other kinetic constants in Eqs. 7 and 8 are listed in the supplementary material Table S2. Note that the soot oxidation by CO_2 and H_2O is assumed to have a similar reaction scheme to that of O_2, which resembles the gasification of char particles. Besides, the soot surface growth caused by the addition of acetylene is not considered in Eq. 7 due to its minor contribution[41] . This effect will be discussed separately in Section 4.

2.3. Computational algorithm

The integrated algorithm that couples the soot formation and the multiphase flow is implemented in the OpenFOAM software[63] . Due to the reason that soot particles are significantly smaller than biomass particles, their inertia can be neglected. Soot is therefore treated as a continuum and its transportation can be described by convection–diffusion-reaction equations in the simulation. Fig. 1 shows the computational process of the integrated algorithm. During the simulation, biomass particles are first injected into the computational domain. Then the particle temperature is solved, based on which pyrolysis and char consumption are computed. In the gas phase, chemical reactions including tar cracking, steam and CO_2 reforming and soot formation are solved. Finally, the source terms in the gas phase governing equations

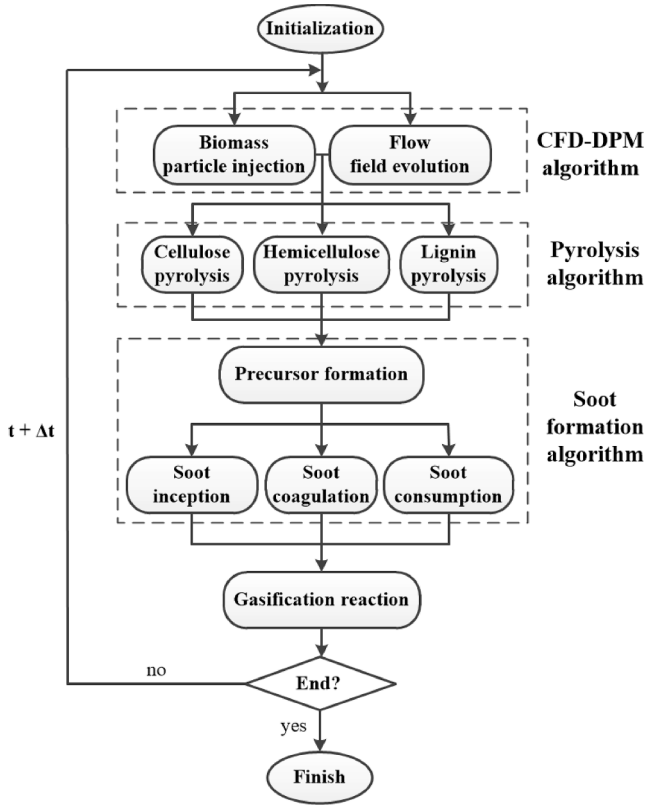

Fig. 1. Coupled CFD-DPM and soot formation algorithm for biomass gasification.

are updated and the convection and diffusion of the flow field are solved. The integrated algorithm is accelerated by using a Massage Passing Interface (MPI) strategy. Unlike the other soot algorithms such as the work of Josephson et al.[41] and Ferreiro et al.[43] , where only the kinetics of soot formation is resolved, the current model is a reactor-scale algorithm that couples the soot formation and flow field evolution. Besides, the biomass pyrolysis is realized by dealing with cellulose, hemicellulose and lignin separately, which enables the study of soot formation for the different components of biomass.

3. Results

Soot formation is a challenging issue in the high-temperature gasification of biomass. Recent experimental studies also show that the soot particles formed during solid fuel gasification have complex internal structures [9], indicating that the intrinsic kinetics is a multiscale problem. However, there is still a lack of comprehensive reactor-scale studies on the role of different sub-processes in soot formation. To achieve this goal, the integrated biomass gasification algorithm is here used to study the soot formation in drop-tube furnaces.

Existing studies illustrate that soot formation in biomass pyrolysis is mainly caused by the tar generation from lignin, while cellulose and hemicellulose only contribute to a small amount of soot. Therefore, it is necessary to make a separate study for the three basic components. Here, we choose the experimental results from Trubetskaya et al., [64] and Deng et al.,[65] to validate the multiphase flow solver in pyrolysis simulations. The experiment of Trubetskaya et al., is carried out in a drop-tube reactor with the operating temperature ranging from 800 to 1250 °C with an isothermal region being 1.06 m long, while in the experiment of Deng et al., the tested temperature is 1300 °C and the length of the isothermal region is 0.6 m.

To validate the model in gasification simulations, the wheat straw gasification experiment carried out by Ferreiro et al. is used for the assessment[43] . The simulation results from the same work are also used for comparison. Note that the gasification and soot formation model in the work of Ferreiro et al. is based on a detailed multistep pyrolysis model[43] , whereas the coupling of the soot formation with the flow field evolution and reaction heat is not fully resolved. In the experiment, the gasification reactor is a drop-tube furnace with an isothermal length of 1750 mm and an inner diameter of 40 mm. There are two groups of experiments. In the first group, the influence of gasification temperature on the soot formation is studied without the addition of steam, while in the second group of the experiments, the gasification temperature is fixed at 1000 °C and the influence of steam/biomass ratio on soot yield is studied.

The biomass material properties and the operating parameters used in the pyrolysis and gasification simulations are provided in the supplementary material Table S3–S6. The current work is mainly focused on the basic kinetics of soot formation. The potential catalytic effects caused by alkali metals are therefore not considered. Besides, due to the

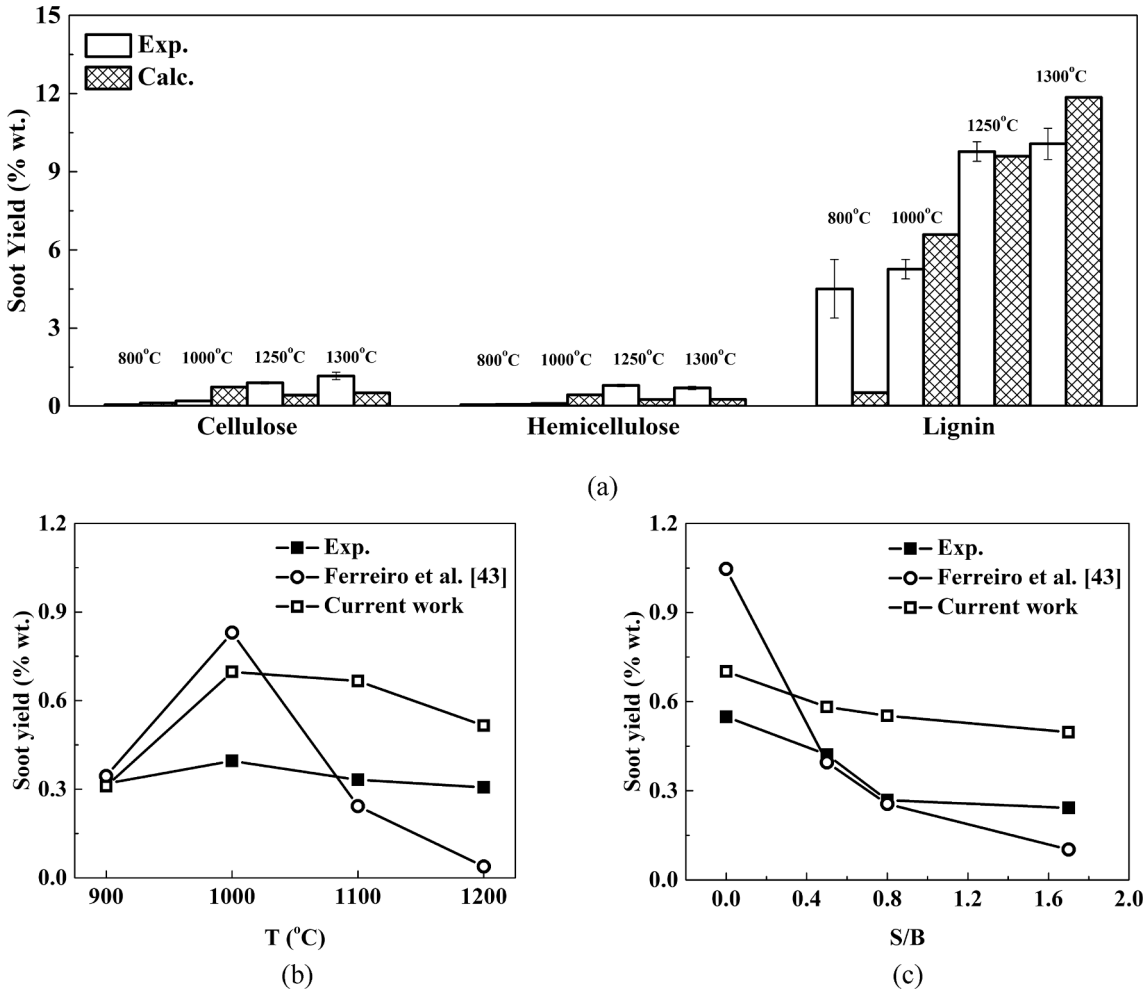

Fig. 2. Comparison of numerical simulation with experimental measurement. (a): Soot yields of cellulose, hemicellulose and lignin pyrolysis (Exp. 800–1250 °C: Trubetskaya et al.[64] ; Exp. 1300 °C: Deng et al.[65]); (b) and (c): Soot yields during wheat straw gasification (Exp.:[43] ; In Fig (c), S/B means steam/biomass ratio and T = 1000 °C).

existence of moisture in the biomass, steam gasification reactions are also considered in the high-temperature pyrolysis simulations. A grid convergency study has been carried out for both the pyrolysis and the gasification cases (Fig. S1 in the supplementary material) to ensure that the numerical results are independent of the spatial discretization adopted.

The computational results of soot yield and the comparison with experimental measurements are presented in Fig. 2. In the pyrolysis simulations (Fig. 2a), the general trend of soot yield for the three basic biomass components is well captured, i.e., the soot produced from cellulose and hemicellulose pyrolysis is far less than that from lignin. In the temperature range of 1000 to 1300 °C, the soot yield from lignin pyrolysis increases from 7% to 12%, which is very close to the experimental observation of 5% to 10%. At 800 °C, the predicted soot yield from lignin is only about 1%, which is a bit lower than the experimental result of 4%. This observation implies that the net soot production mechanism at a relatively low temperature might be different from that at higher temperatures. Actually, recent theoretical computations have shown evidence that the soot formation at low temperatures is likely to be dominated by a physical agglomeration process rather than a chemical reaction process such as HACA [66–68]. With molecular dynamics simulations, Mao and Yuan et al. demonstrated that soot precursors can agglomerate by van der Waals forces without forming covalent bonds at relatively low temperatures [66,67]. With the increase of temperature, the physical nucleation is overtaken by chemical nucleation where covalent bonds are likely to form. However, the physical nucleation mechanism is not modeled in the current work, instead, our primary focus is rather on the high-temperature situation (above 1000 °C) which is a typical operating condition for soot generation. For the results of cellulose and hemicellulose, the predicted soot yield lies in the same order of magnitude as the experimental observation. Besides, the soot yield from cellulose pyrolysis is a little bit higher than that of hemicellulose, which is also observed in the experiment.

Fig. 2b shows the soot formation in the gasification simulations under different operating temperatures. The two predicted soot products at 900 °C are very close to the experimental result (~0.3%). At 1000 °C, the soot yield in our simulation increases to 0.8%, which shows a similar overprediction with that of Ferreiro et al. compared with the experimental data (~0.4%). When the operating temperature exceeds 1000 °C, the soot yield in the current work exhibits a slightly decreased trend that is close to the experimental measurement, although the final soot yield (0.5%) is still larger than the experimental result (0.3%). On the other hand, the predicted soot in the work of Ferreiro et al. sees a rapid decrease after 1000 °C, and almost vanishes at 1200 °C. Note that, the soot particle size distribution is not resolved in the work of Ferreiro et al., while in the current work, the transport of the soot mass fraction and the soot particle number density are both included. Besides, the reaction heat of gasification reactions is also accounted for within the CFD solver. The comparison demonstrates that, although a simplified one-step global type pyrolysis model is used in our work, the trend of soot generation is still well captured, given that the coupling of the soot formation with the flow-field evolution and the chemical reactions is properly modeled.

In the second group of the gasification experiments, the influence of the steam/biomass (S/B) ratio on the soot formation is studied. Fig. 2c compares the soot yield with that from the experiment and the simulation result of Ferreiro et al. It is shown that the predicted soot yield at S/B = 0 is about 0.7%, which is very close to the experimental data of 0.5%. However, the result of Ferreiro et al. is nearly doubled to the experimental measurement. When S/B increases to 0.5, a decrease of 0.1 percentage units in soot yield is seen in the current work, which shows a similar trend as the experiment. However, the model of Ferreiro et al. predicts a very rapid drop in the soot product. The difference between the two predictions is mainly caused by the different soot oxidation models used in the simulation. In Ferreiro et al., the soot is consumed by a gas phase reaction model, while in the current work, soot oxidation only happens on the surface of soot particles, which is a much slower process than that with a gas-phase reaction model[41] . For the same reason, the soot consumption does not show a significant increase with increasing the steam/biomass ratio, resulting in a higher soot yield in the current work. However, the general trend of the soot yield in our simulations corresponds well with the experimental result.

To get a clear understanding of the pyrolysis and gasification processes, Fig. 3 shows the steady-state distribution of soot mass fraction and the average soot particle size in the drop-tube furnace along with the biomass and char particle distribution for cellulose and lignin pyrolysis. The comparison is made between 1000 °C and 1300 °C. Note that an extra 10 cm in reactor length is added above the biomass injection position in the simulation to avoid the influence of the inflow boundary conditions. It is observed that the injected biomass particles undergo a fast heating and pyrolysis process at 1000 °C. Soot formation can be seen immediately after devolatilization for lignin pyrolysis. Besides, the soot mass fraction in the near-wall region is slightly higher than that in the center area. This is mainly due to the lower velocity of the gas in this region, indicating that soot formation is closely coupled to the convection and diffusion processes in the flow field. At 1300 °C, the soot formation becomes faster and happens almost immediately after the injection of the biomass. At the same time, the chemical reactions are also promoted in this high-temperature condition, for example, the consumption reactions of tar and soot by the steam generated during the pyrolysis process, which result in the reduction of soot generation. For the lignin case, the soot mass fraction increases rapidly after a short period of tar cracking. Due to the large amount of tar generated from the pyrolysis, the soot generation at 1300 °C is very fast, resulting in a higher mass fraction in the center area than that in the near-wall region.

The soot particle size distribution is also shown in Fig. 3. At 1000 °C, the soot particles in the pyrolysis of both cellulose and lignin grow slowly along the reactor with a final size reaching around 20 nm at the reactor exit. With the temperature increasing to 1300 °C, the soot particle size increases rapidly due to the accumulation of a higher amount of soot that has been generated. For the cellulose component, the soot particle size increases to about 20 nm very fast after the initial nucleation, which is followed by a longer agglomeration process where the soot particle size reaches around 40 nm. For the lignin component, the average soot particle size stays around 100 nm in the outlet of the furnace at 1300 °C. In the experiment[64] , the reported average soot particle size for the cellulose pyrolysis is about 35 nm with a maximum value of 115 nm at 1250 °C, while the data for the lignin pyrolysis are 45 nm on average and 120 nm at the maximum, respectively. The deviation in the predicted soot particle size distribution from experimental measurement may have many explanations. One likely aspect is due to the simplification made for the sub-processes of soot formation in the modeling. For example, the adopted resolution on only the average soot particle size makes it effectively difficult to accurately model soot particle growth due to interactions of entities of different sizes within one computational cell. Besides, the coupling between the soot formation and the flow field evolution might also cause a certain impact. This analysis demonstrates that there is still a long way to go to develop a soot formation model that produces accurate predictions of both mass and particle size for biomass gasification. The differences in soot particle size distribution between simulations and experiments may influence the prediction of the soot consumption during gasification, as the consumption has a close relationship with the surface area of the soot particles. This issue will be further discussed in the following section.

Fig. 4 shows the soot mass fraction and particle size contours for the gasification simulations at different operating temperatures. Fig. 4a illustrates that, under a relatively low temperature of 900 °C, the soot mass fraction has a nearly uniform distribution along the radial direction inside the furnace. However, with the increase of temperature, soot formation becomes faster, resulting in a higher soot mass fraction in the center area. At 1200 °C, there is an apparent core region in the initial soot formation stage with a high soot mass fraction. At longer distances,

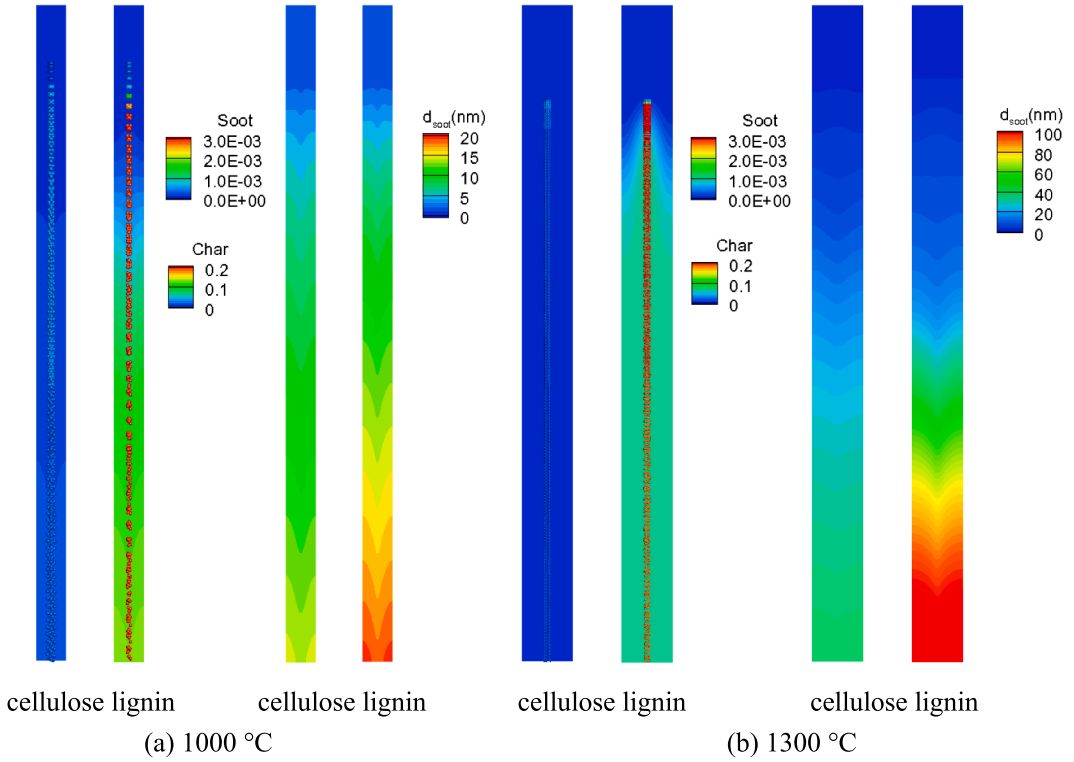

Fig. 3. Soot mass fraction ("Soot", background color) and soot particle size distributions ("d_{soot}") during the pyrolysis of cellulose and lignin: (a) 1000 °C: simulation of the experiment of Trubetskaya et al. [64]; (b) 1300 °C: simulation of the experiment of Deng et al. [65].

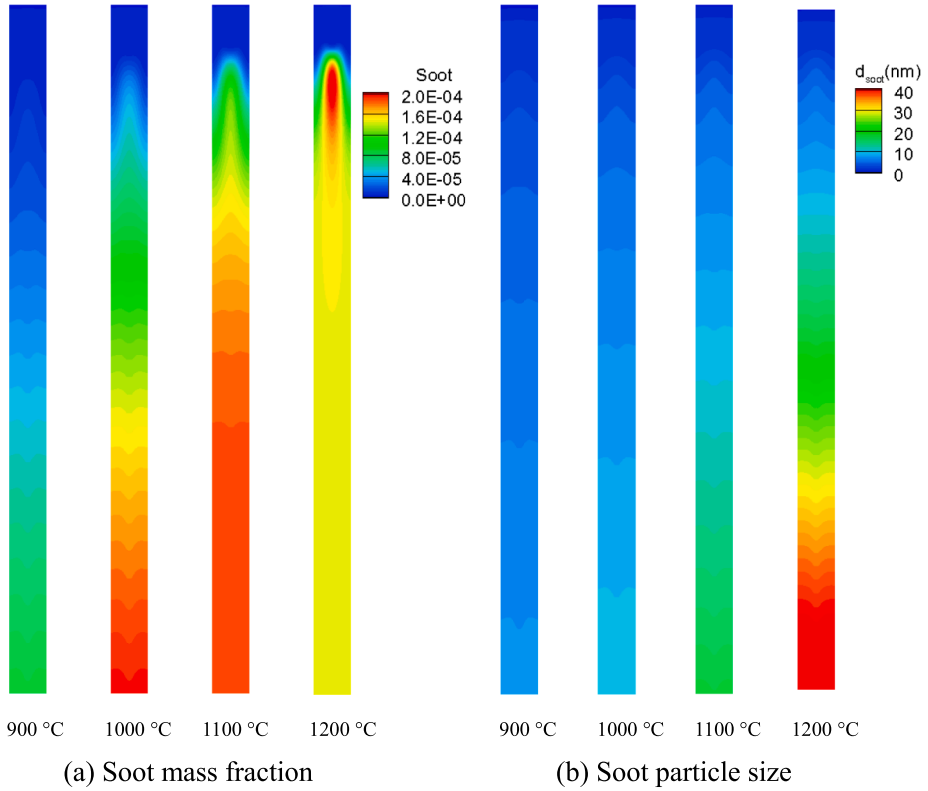

Fig. 4. Soot yields (mass fraction, "Soot", and particle size "d_{soot}") at different gasification temperatures (the displayed furnace length is scaled down by a factor of 2.5).

the soot diffuses in the radial direction. The mass fraction contour demonstrates that the convection and diffusion of soot is an important factor that might well influence the prediction accuracy. Fig. 4b shows that the soot particle size distribution is quite different from its mass fraction, in that it exhibits a nearly uniform distribution in the radial direction for all the cases studied.

Besides the above results, additional information including gas products and species distributions are also provided in the supplementary material (Figs. S2–S6). The comparison illustrates that the reactor-scale soot formation algorithm reaches an overall good agreement with experimental results in both pyrolysis and gasification.

4. Discussion

As shown in the analyses presented throughout the previous section, soot mainly comes from the lignin content in biomass. Furthermore, the soot formation process is accompanied by the competition of tar/soot conversion and oxidation during biomass gasification. The flow field evolution has a non-trivial effect on the spatial and temporal species distributions, chemical reactions and thus also the soot generation. Therefore, it is necessary to make a comprehensive investigation on the impact of the different influential factors.

4.1. Influence of tar consumption on soot formation

Tar plays an important role in soot formation. Owning to the use of a simplified tar evolution model, it becomes straightforward to study the competition of tar consumption and conversion. Fig. 5a compares the soot yield with and without considering the oxidation of tar (lumped as $C_6H_{6.2}O_{0.2}$ in this work) with O_2, H_2O and CO_2. It is seen that tar consumption significantly reduces the soot yield by almost two-thirds. If tar consumption is not considered, the soot yield reaches 1.6% at 1000 °C, while it decreases to 0.6% in the real case that accounts for the consumption reactions. A similar influence on the soot yield is also seen for the 1100 °C case. When the operating temperature further increases to 1200 °C, tar cracking reaction is also promoted. As a result, the relative impact of tar consumption becomes weaker. The soot mass fraction (Fig. 5a2) and tar distribution (Fig. S7 in supplementary material) further show the difference with and without considering tar consumption reactions. It is clearly seen that tar conversion is very fast and confined to a small region near the injection (0–0.2 m). In addition, a relatively larger amount of tar is consumed by the gasifying agent rather than converting to soot at 1100 °C with the steam/biomass ratio of 0.5. The influence of tar consumption on soot particle size evolution is shown in Fig. 5a3. When the consumption reactions are not considered, all of

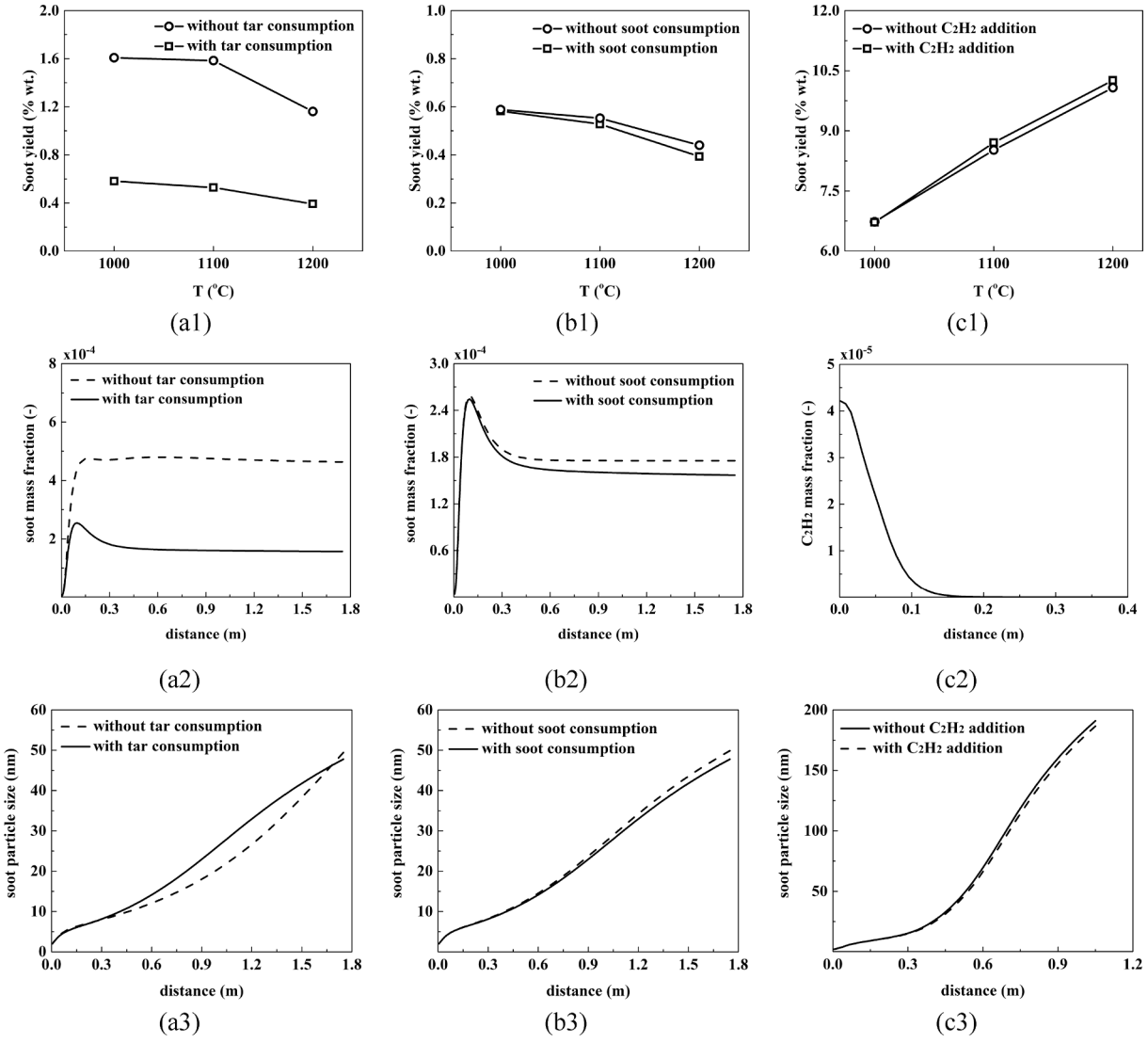

Fig. 5. Influence of tar consumption, soot consumption and surface growth on soot yields and soot particle size distribution along the centerline of the reactor at T = 1200 °C. (a) and (b): gasification with S/B = 0.5; (c) softwood lignin pyrolysis.

the tar converts to soot resulting in a tendency to create more and larger incipient soot particles. However, the soot consumption is also promoted due to the increased soot particle surface area at the high operating temperature of 1200 °C. Therefore, after 0.4 m, the soot particle size predicted without considering tar consumption shows a slower increasing trend compared with that of the real situation. From about 1.0 m, coagulation becomes dominant again in the growth of the soot particles. As a result, the final predicted soot particle size at the exit of the reactor is essentially identical to that of the original case (Fig. 5a3).

4.2. Influence of soot consumption rate on soot formation

Unlike the work of Ferreiro et al., the soot consumption in this work is computed based on the surface oxidation by O_2, H_2O, and CO_2 of soot particles, which captures the soot consumption more reasonably than a gas-phase consumption model. However, existing studies have shown that soot oxidation is a complex process depending on the internal structures of soot particles which is closely related to the fuel type and soot formation history[32] [35,36]. Therefore, it is necessary to study the influence of soot consumption separately. Fig. 5b compares the predicted soot yield with and without considering soot consumption by O_2, H_2O and CO_2. It is shown that the impact of the soot oxidation reactions is negligible at 1000 °C. With the increase of operating temperature, the effect of soot oxidation becomes stronger. At 1200 °C, the oxidation reactions reduce the soot yield by around 10%. The soot distribution in Fig. 5b2 illustrates that soot consumption mainly happens after the initial nucleation stage beyond 0.3 m of the biomass injection position, where soot mixes uniformly with the gasifying agent. The effect on the predicted final soot particle size is again small (Fig. 5b3). Besides, it is also observed that soot consumption is a relatively slow process compared with the nucleation process.

4.3. Influence of surface growth on soot formation

Existing studies have shown that surface growth through the HACA mechanism is a common way of mass build-up for soot particles [45,48,60]. However, in the work of Josephson et al.[41] , it was found that the effect of surface growth and consumption is quite small compared with that of precursor nucleation due to the small amount of C_2H_2 generated during pyrolysis. Actually, it is found that the acetylene yield during primary pyrolysis is less than 0.003%, while for tar cracking the value is about 0.5% [69] . Therefore, acetylene is usually not considered in biomass pyrolysis mechanisms even in some detailed pyrolysis models [21]. In our simplified model, only coagulation is considered for the growth of soot particles. To critically access this modeling choice, the effect of surface growth on soot formation is analyzed separately in this subsection based on the pyrolysis simulation of the softwood lignin studied in Section 3 (the simulation case for the experiment of Trubetskaya et al. [64]). Here we assume that acetylene with a mass flow rate accounting for 0.15% of the lignin feeding rate is added directly into the furnace (assuming a maximum of 30% tar generation from lignin pyrolysis). The surface growth of soot particles is then realized by the carbon addition reaction $C_2H_2 \rightarrow 2C + H_2$, where the reaction rate is determined as [45,60]: $k_{sgs} = C_{sgs}[X_{C2H2}]exp(-\frac{T_{sgs}}{T})\cdot(\pi N)^{\frac{1}{3}}\left(\frac{6M}{\rho_{soot}}\right)^{\frac{2}{3}}$.

Fig. 5c compares the soot generation with and without (base case) considering surface growth caused by acetylene. It is shown that the surface growth reaction only slightly increases the soot yield at the operating temperature higher than 1100 °C due to the small amount of acetylene added to the reactor. Fig. 5c2 and 5c3 present the C_2H_2 and soot particle size distribution along the centerline of the furnace. One can see that the consumption of acetylene is very fast at 1200 °C and that it finishes within a short range of 0–0.2 m. The surface growth reaction increases the initial soot particle size. The coagulation rate of incipient soot particles is therefore also accelerated (Eq. 8). As a result, the total number of soot particles is relatively reduced in the surface growth region (0–0.2 m) compared with that of the base case, which in turn decreases the coagulation rate in the subsequent reaction path from 0.2 to 1.06 m. Therefore, the final soot particle size considering surface growth is slightly reduced compared with the base case.

4.4. Uncertainty of soot yields with lignin content variation

Lignin is the main source of soot yield during biomass gasification, which is simplified with a combination of $C_{15}H_{14}O_4$ (ligC), $C_{20}H_{22}O_{10}$ (ligO), and $C_{22}H_{28}O_9$ (ligH) in this study. Unlike cellulose and hemicellulose, lignin is a complex polymer and its mass fraction can differ a lot even for the same type of biomass due to the compound nature of biomass materials. To make an uncertainty analysis of the impact of the variation in lignin content, soot yields with different lignin components in the biomass are studied. Fig. 6a shows the soot yield with lignin mass fraction increases from 12% to 17% and 22% (dry basis), while the mass fractions of cellulose and hemicellulose are reduced accordingly by keeping the same mass ratio. In Fig. 6b, the mass fractions of lignin are fixed the same of 17% while the lignin composition is replaced by the ligC, ligH, and ligO, respectively. The 17% lignin content is set as the base case, which is studied in the previous gasification simulations (the mass fractions of ligC, ligH and ligO in the base case are listed in Table S6 in the supplementary material). The other operating conditions are set the same as in the base case. It is shown that, with an increase of 5% in lignin content, the relative soot yield increases by about 15% for operating temperatures in the interval of 1000 to 1200 °C (Fig. 6a1). Fig. 6a2 compares the soot distribution in the reactor with different lignin mass contents. It is observed that the mass fraction shows a similar evolution trend for the three cases studied, which is around 2.0e-4 in the center line of the reactor. For the soot particle size distribution (Fig. 6a3), on the other hand, only a small influence is caused with a 5% increase of lignin content, indicating that the increase of soot particle size is not proportional to that of the lignin mass content. Instead, it is a combined result of agglomeration and consumption. The final cell-averaged soot particle size at the outlet of the reactor (distance = 1.75 m) reaches around 18 nm for all the tested cases. Fig. 6b illustrates that the composition of lignin also has a non-negligible influence on the soot formation. The predicted soot yields with replacing the lignin compound by its three basic components are ligC > ligH > ligO, where the variation is about 10% around the base case. The soot mass fraction (Fig. 6b2) and soot particle size (Fig. 6b3) distributions show a similar increase/decrease trend with that of the soot yield (Fig. 6b1).

5. Conclusions

A new biomass gasification model is established by integrating an Eulerian-Lagrangian multiphase flow algorithm with a two-equation soot formation model that considers the evolution of both soot mass fraction and soot particle size. The soot generation is modeled in a simplistic yet straightforward manner, and the complete model framework accounts for the most important sub-processes, including the formation and cracking of tar, the nucleation of soot particles, and the consumption reactions of tar and soot. The integrated model captures the coupling of soot formation with the flow-field evolution and chemical reactions, which enables a comprehensive study of the soot generation in complex biomass gasification at reactor scale.

The integrated model is first validated by pyrolysis experiments of the three basic biomass components, cellulose, hemicellulose, and lignin at a temperature range from 800 to 1300 °C. The predicted soot yields are around 1% for cellulose and hemicellulose and 10% for softwood lignin, which correspond well with the experimental measurement. Besides, the general trend of soot yield with temperature is also well captured for the lignin component, which is a major source of soot formation in the pyrolysis of biomass. Thereafter, the model is used to

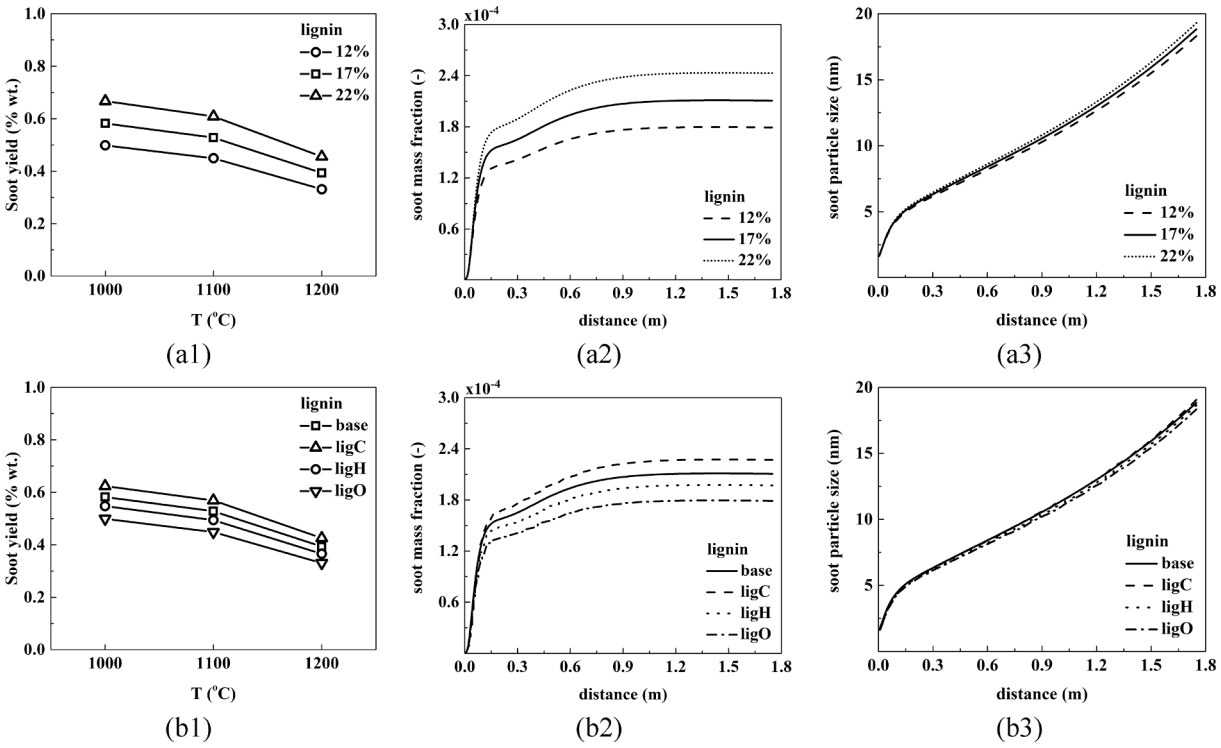

Fig. 6. Sensitivity of the soot yields and soot particle size distribution along the centerline of the reactor to the variation of the lignin content (dry basis) in the biomass during gasification (in (a1) and (b1) S/B = 0.5; in (a2), (a3), (b2) and (b3) T = 1100 °C, S/B = 0.5).

simulate biomass steam gasification in a drop-tube furnace. The current work performs better than an alternate model that is based on a detailed pyrolysis model without consideration of the soot particle size distribution and the flow-field evolution at varying operating temperatures and steam/biomass ratios. However, the predicted soot particle size distribution is not fully in line with that of experimental results, indicating certain limitations of the classical two-equation soot model for the current class of problems.

The simulations reveal the important coupling between the flow-field evolution, chemical reactions, and soot generation. More specifically, a non-uniform distribution of soot is observed in the furnace at high temperatures caused by the interaction of soot formation and transport. A sensitivity study shows that tar consumption has a significant influence on soot formation, which would triple the soot yield if the reactions of tar oxidation were not considered. Furthermore, the impact of soot consumption on the soot yield becomes stronger with the increase of operating temperature and reaches 10% at 1200 °C. The surface growth effect caused by the HACA mechanism only slightly increases the soot yield without considerably altering the soot particle size due to the small amount of acetylene generated from pyrolysis (0.15%). Finally, the influence caused by the variation of lignin content is also studied. It is found that a 5% increase in lignin mass content results in a relatively 15% promotion of the soot yield. Besides, the uncertainty of soot yield caused by the variation of the lignin component could exceed 10%.

CRediT authorship contribution statement

Tao Chen: Conceptualization, Methodology, Software, Validation, Writing - original draft. **Tian Li:** Conceptualization, Formal analysis, Investigation, Writing - review & editing. **Jonas Sjöblom:** Formal analysis, Writing - review & editing. **Henrik Ström:** Conceptualization, Funding acquisition, Investigation, Methodology, Writing - review & editing.

Declaration of Competing Interest

The authors declare that they have no known competing financial interests or personal relationships that could have appeared to influence the work reported in this paper.

Acknowledgements

This work is financially supported by the Swedish Energy Agency (No. 46439-1), the Swedish Research Council Formas (No. Dnr 2017-00677), the Research Council of Norway (GASPRO, No. 267916), the Swedish Centre for Biomass Gasification (SFC, No. P34721-3) and the Centre for Combustion Science and Technology (CECOST). The computations were enabled by resources provided by the Swedish National Infrastructure for Computing (SNIC) partially funded by the Swedish Research Council through grant agreement no. 2018-05973.

Appendix A. Supplementary data

Supplementary data to this article can be found online at https://doi.org/10.1016/j.fuel.2021.121240.

References

[1] Scheftelowitz M, Becker R, Thrän D. Improved power provision from biomass: a retrospective on the impacts of German energy policy. Biomass Bioenergy 2018;111:1–12.
[2] Bogush AA, Stegemann JA, Williams R, Wood IG. Element speciation in UK biomass power plant residues based on composition, mineralogy, microstructure and leaching. Fuel 2018;211:712–25.
[3] Jåstad EO, Bolkesjø TF, Trømborg E, Rørstad PK. The role of woody biomass for reduction of fossil GHG emissions in the future North European energy sector. Appl Energy 2020;274:115360.
[4] Ashok J, Dewangan N, Das S, Hongmanorom P, Wai MH, Tomishige K, et al. Recent progress in the development of catalysts for steam reforming of biomass tar model reaction. Fuel Process Technol 2020;199:106252.
[5] Albashabsheh NT, Heier Stamm JL. Optimization of lignocellulosic biomass-to-biofuel supply chains with densification: literature review. Biomass Bioenergy 2021;144:105888. https://doi.org/10.1016/j.biombioe.2020.105888.

[6] Ren J, Cao J-P, Zhao X-Y, Yang F-L, Wei X-Y. Recent advances in syngas production from biomass catalytic gasification: a critical review on reactors, catalysts, catalytic mechanisms and mathematical models. Renew Sustain Energy Rev 2019;116:109426. https://doi.org/10.1016/j.rser.2019.109426.

[7] Zabrodiec D, Massmeyer A, Hees J, Hatzfeld O, Kneer R. Flow pattern and behavior of 40 kWth pulverized torrefied biomass flames under atmospheric and oxy-fuel conditions. Renew Sustain Energy Rev 2021;138:110493. https://doi.org/10.1016/j.rser.2020.110493.

[8] Tremel A, Becherer D, Fendt S, Gaderer M, Spliethoff H. Performance of entrained flow and fluidised bed biomass gasifiers on different scales. Energy Convers Manage 2013;69:95–106.

[9] He Q, Guo Q, Umeki K, Ding Lu, Wang F, Yu G. Soot formation during biomass gasification: a critical review. Renew Sustain Energy Rev 2021;139:110710. https://doi.org/10.1016/j.rser.2021.110710.

[10] Koziński JA, Saade R. Effect of biomass burning on the formation of soot particles and heavy hydrocarbons. An experimental study. Fuel 1998;77(4):225–37.

[11] Umeki K, Häggström G, Bach-Oller A, Kirtania K, Furusjö E. Reduction of tar and soot formation from entrained-flow gasification of woody biomass by alkali impregnation. Energy Fuels 2017;31(5):5104–10.

[12] Wu Z, Wang S, Zhao J, Chen L, Meng H. Product distribution during co-pyrolysis of bituminous coal and lignocellulosic biomass major components in a drop-tube furnace. Energy Fuels 2015;29(7):4168–80.

[13] Trubetskaya A, Souihi N, Umeki K. Categorization of tars from fast pyrolysis of pure lignocellulosic compounds at high temperature. Renew Energy 2019;141:751–9.

[14] Nguyen HNT, Seemann M, Thunman H. Fate of polycyclic aromatic hydrocarbons during tertiary tar formation in steam gasification of biomass. Energy Fuels 2018;32(3):3499–509.

[15] Matamba T, Tahmasebi A, Rish SK, Yu J. Understanding the enhanced production of poly-aromatic hydrocarbons during the pyrolysis of lignocellulosic biomass components under pressurized entrained-flow conditions. Fuel Process Technol 2021;213:106645.

[16] Font Palma C. Model for biomass gasification including tar formation and evolution. Energy Fuels 2013;27(5):2693–702.

[17] Gómez-Barea A, Leckner B. Modeling of biomass gasification in fluidized bed. Prog Energy Combust Sci 2010;36:444–509.

[18] Wang S, Dai G, Yang H, Luo Z. Lignocellulosic biomass pyrolysis mechanism: a state-of-the-art review. Prog Energy Combust Sci 2017;62:33–86.

[19] Morf P. Secondary reactions of tar during thermochemical biomass conversion. Ph. D. thesis. Swiss Federal Institute of Technology 2002.

[20] Ranzi Eliseo, Cuoci Alberto, Faravelli Tiziano, Frassoldati Alessio, Migliavacca Gabriele, Pierucci Sauro, et al. Chemical kinetics of biomass pyrolysis. Energy Fuels 2008;22(6):4292–300.

[21] Debiagi Paulo Eduardo Amaral, Pecchi Chiara, Gentile Giancarlo, Frassoldati Alessio, Cuoci Alberto, Faravelli Tiziano, et al. Extractives extend the applicability of multistep kinetic scheme of biomass pyrolysis. Energy Fuels 2015;29(10):6544–55.

[22] Gentile G, Debiagi PEA, Cuoci A, Frassoldati A, Ranzi E, Faravelli T. A computational framework for the pyrolysis of anisotropic biomass particles. Chem Eng J 2017;321:458–73.

[23] Chen Tao, Ku Xiaoke, Li Tian, Karlsson Bodil SA, Sjöblom Jonas, Ström Henrik. High-temperature pyrolysis modeling of a thermally thick biomass particle based on an MD-derived tar cracking model. Chem Eng J 2021;417:127923. https://doi.org/10.1016/j.cej.2020.127923.

[24] Debiagi Paulo Eduardo Amaral, Gentile Giancarlo, Pelucchi Matteo, Frassoldati Alessio, Cuoci Alberto, Faravelli Tiziano, et al. Detailed kinetic mechanism of gas-phase reactions of volatiles released from biomass pyrolysis. Biomass Bioenergy 2016;93:60–71.

[25] Ahrenfeldt Jesper, Egsgaard Helge, Stelte Wolfgang, Thomsen Tobias, Henriksen Ulrik Birk. The influence of partial oxidation mechanisms on tar destruction in two stage biomass gasification. Fuel 2013;112:662–80.

[26] Feng Dongdong, Zhao Yijun, Zhang Yu, Sun Shaozeng. Effects of H_2O and CO_2 on the homogeneous conversion and heterogeneous reforming of biomass tar over biochar. Int J Hydrogen Energy 2017;42(18):13070–84.

[27] Horvat A. A study of the uncertainty associated with tar measurement and an investigation of tar evolution and composition during the air-blown fluidised bed gasification of torrefied and nontorrefied grassy biomass. Ph.D. thesis. University of Limerick; 2016.

[28] Commodo Mario, Kaiser Katharina, De Falco Gianluigi, Minutolo Patrizia, Schulz Fabian, D'Anna Andrea, et al. On the early stages of soot formation: molecular structure elucidation by high-resolution atomic force microscopy. Combust Flame 2019;205:154–64.

[29] Brookes S, Moss J. Predictions of soot and thermal radiation properties in confined turbulent jet diffusion flames. Combust Flame 1999;116(4):486–503.

[30] Rigopoulos Stelios. Modelling of soot aerosol dynamics in turbulent flow. Flow Turbul Combust 2019;103(3):565–604.

[31] Deng C, Wu H. Mechanistic insights into effect of feeding rate on soot formation during rapid pyrolysis of biomass model components in a drop-tube furnace at high temperature. Proc Combust Inst 2020;000:1–9.

[32] Chang Qinghua, Gao Rui, Gao Ming, Yu Guangsuo, Mathews Jonathan P, Wang Fuchen. Experimental analysis of the evolution of soot structure during CO_2 gasification. Fuel 2020;265:116699. https://doi.org/10.1016/j.fuel.2019.116699.

[33] Pejpichestakul Warumporn, Frassoldati Alessio, Parente Alessandro, Faravelli Tiziano. Kinetic modeling of soot formation in premixed burner-stabilized stagnation ethylene flames at heavily sooting condition. Fuel 2018;234:199–206.

[34] Morán José, Poux Alexandre, Yon Jérôme. Impact of the competition between aggregation and surface growth on the morphology of soot particles formed in an ethylene laminar premixed flame. J Aerosol Sci 2021;152:105690. https://doi.org/10.1016/j.jaerosci.2020.105690.

[35] Davis Justin, Molnar Eric, Novosselov Igor. Nanostructure transition of young soot aggregates to mature soot aggregates in diluted diffusion flames. Carbon 2020;159:255–65.

[36] Chang Qinghua, Gao Rui, Gao Ming, Yu Guangsuo, Wang Fuchen. The structural evolution and fragmentation of coal-derived soot and carbon black during high-temperature air oxidation. Combust Flame 2020;216:111–25.

[37] Wiinikka Henrik, Toth Pal, Jansson Kjell, Molinder Roger, Broström Markus, Sandström Linda, et al. Particle formation during pressurized entrained flow gasification of wood powder: effects of process conditions on chemical composition, nanostructure, and reactivity. Combust Flame 2018;189:240–56.

[38] Trubetskaya A, Jensen PA, Jensen AD, Llamas ADG, Umeki K, Gardini D, et al. Effects of several types of biomass fuels on the yield, nanostructure and reactivity of soot from fast pyrolysis at high temperatures. Appl Energy 2016;171:468–82.

[39] Yu J, Guo Q, Gong Y, Ding L, Wang J, Yu G. A review of the effects of alkali and alkaline earth metal species on biomass gasification. Fuel Process Technol 2021;214:106723.

[40] Brown Alexander L, Fletcher Thomas H. Modeling soot derived from pulverized coal. Energy Fuels 1998;12(4):745–57.

[41] Josephson Alexander J, Linn Rod R, Lignell David O. Modeling soot formation from solid complex fuels. Combust Flame 2018;196:265–83.

[42] Niksa Stephen. Predicting ultimate soot yields from any coal. Proc Combust Inst 2019;37(3):2757–64.

[43] Ferreiro AI, Segurado R, Costa M. Modelling soot formation during biomass gasification. Renew Sustain Energy Rev 2020;134:110380. https://doi.org/10.1016/j.rser.2020.110380.

[44] Xu Kailong, Wu Yuxin, Shen Haoshu, Zhang Qi, Zhang Hai. Predictions of soot formation and its effect on the flame temperature of a pulverized coal-air turbulent jet. Fuel 2017;194:297–305.

[45] Muto Masaya, Yuasa Kohei, Kurose Ryoichi. Numerical simulation of soot formation in pulverized coal combustion with detailed chemical reaction mechanism. Adv Powder Technol 2018;29(5):1119–27.

[46] Takahashi H, Hashimoto N, Watanabe H, Kurose R, Fujita O. Prediction of soot formation characteristics in a pulverized-coal combustion field by large eddy simulations with the TDP model. Proc Combust Inst 2019;37:2883–91.

[47] Richter H, Granata S, Green WH, Howard JB. Detailed modeling of PAH and soot formation in a laminar premixed benzene/oxygen/argon low-pressure flame. Proc Combust Inst 2005;30:1397–405.

[48] Frenklach M, Wang H. Detailed mechanism and modeling of soot particle formation. In: Soot formation in combustion. Springer-Verlag; 1994. p. 165–92.

[49] Josephson AJ. Modeling soot formation derived from solid fuels. Ph.D. thesis. Brigham Young University; 2018.

[50] Vishwanathan G, Reitz RD. Development of a practical soot modeling approach and its application to low-temperature diesel combustion. Combust Sci Tech 2010;182:1050–82.

[51] Josephson Alexander J, Hopkins Emily M, Lignell David O, Linn Rod R. Reduction of a detailed soot model for simulations of pyrolysing solid fuels. Combust Theory Modell 2020;24(1):15–40.

[52] Lu Hong, Robert Warren, Peirce Gregory, Ripa Bryan, Baxter Larry L. Comprehensive study of biomass particle combustion. Energy Fuels 2008;22(4):2826–39.

[53] Chen Tao, Ku Xiaoke, Lin Jianzhong, Fan Liwu. New pyrolysis model for biomass particles in a thermally thick regime. Energy Fuels 2018;32(9):9399–414.

[54] Chen T, Ku X, Lin J, Jin H. Modeling of combustion for thermally thick biomass particles. Powder Technol 2019;353:110–24.

[55] Ku Xiaoke, Li Tian, Løvås Terese. Eulerian-Lagrangian simulation of biomass gasification behavior in a high-temperature entrained-flow reactor. Energy Fuel 2014;28(8):5184–96.

[56] Ngamsidhiphongsa N, Ponpesh P, Shotipruk A, Arpornwichanop A. Analysis of the Imbert downdraft gasifier using a species-transport CFD model including tar-cracking reactions. Energy Convers Manage 2020;213:112808.

[57] Blondeau Julien, Jeanmart Hervé. Biomass pyrolysis at high temperatures: prediction of gaseous species yields from an anisotropic particle. Biomass Bioenergy 2012;41:107–21.

[58] Salem Ahmed M, Zaini Ilman Nuran, Paul Manosh C, Yang Weihong. The evolution and formation of tar species in a downdraft gasifier: numerical modelling and experimental validation. Biomass Bioenergy 2019;130:105377. https://doi.org/10.1016/j.biombioe.2019.105377.

[59] Salem Ahmed M, Paul Manosh C. An integrated kinetic model for downdraft gasifier based on a novel approach that optimises the reduction zone of gasifier. Biomass Bioenergy 2018;109:172–81.

[60] ANSYS Fluent Theory Guide 2013. 15th release, ANSYS Inc., Canonsburg, Pennsylvani.

[61] Hall RJ, Smooke MD, Colket MB. Physical and chemical aspects of combustion. Gordon Breach 1997.

[62] Ong JC. Development of Lagrangian soot tracking method for the study of soot morphology in diesel spray combustion. PhD thesis. University of Nottingham; 2017.

[63] OpenCFD Ltd. OpenFOAM-The open source CFD toolbox-user guide (Version2.1.1). 2012.

[64] Trubetskaya A, Timko MT, Umeki K. Prediction of fast pyrolysis products yields using lignocellulosic compounds and ash contents. Appl Energy 2020;257:113897.

[65] Deng Changya, Liaw Sui Boon, Gao Xiangpeng, Wu Hongwei. Differences in soot produced from rapid pyrolysis of xylan, cellulose and lignin under pulverized-fuel conditions. Fuel 2020;265:116991. https://doi.org/10.1016/j.fuel.2019.116991.
[66] Mao Qian, van Duin Adri CT, Luo KH. Formation of incipient soot particles from polycyclic aromatic hydrocarbons: a ReaxFF molecular dynamics study. Carbon 2017;121:380–8.
[67] Yuan H, Kong W, Liu F, Chen D. Study on soot nucleation and growth from PAHs and some reactive species at flame temperatures by ReaxFF molecular dynamics. Chem Eng Sci 2019;195:748–57.
[68] Frenklach M, Mebel AM. On the mechanism of soot nucleation. PCCP 2020;22:5314.
[69] Guizani Chamseddine, Valin Sylvie, Billaud Joseph, Peyrot Marine, Salvador Sylvain. Biomass fast pyrolysis in a drop tube reactor for bio oil production: experiments and modeling. Fuel 2017;207:71–84.